ACS EARTH AND SPACE CHEMISTRY

Article

Cite This: ACS Earth Space Chem. 2019, 3, 2404−2414

http://pubs.acs.org/journal/aesccq

Atmospheric Processes of Aromatic Hydrocarbons in the Presence of Mineral Dust Particles in an Urban Environment

Zechen Yu and Myoseon Jang*

Department of Environmental Engineering Sciences, University of Florida, Gainesville, Florida 32611, United States

Supporting Information

ABSTRACT: The impact of Gobi Desert dust (GDD) particles on the secondary organic aerosol (SOA) formation was studied to understand the photooxidation of volatile organic compounds, namely, toluene, 1,3,5-trimethylbenzene, and gasoline vapor, in the presence of NO_x using a large outdoor photochemical smog chamber under natural sunlight. SOA yields of all three precursors were found to significantly increase in the presence of GDD particles. The mechanistic role of mineral dust in SOA growth changed with the dust-phase water content. In the presence of dry dust, the formation of carboxylate salts increased SOA growth, but it was limited by the dust's buffering capacity associated with the quantity of alkaline carbonates that react with carboxylic acids. In the presence of wet GDD particles, the pathway via aqueous reactions of oxygenated organic products enhanced SOA growth. Nitric acid absorbed on wet GDD particles suppressed gas-dust partitioning of weakly acidic carboxylic acids. The formation of alkaline carboxylates was also supported by Fourier transform infrared spectroscopy of the SOA formed in the presence of dry GDD. The partitioned SOA products can be further oxidized by dust-phase OH radicals generated by photoactivation of semiconducting metal oxides (i.e., TiO_2). This heterogeneous oxidation of SOA products was observed by studying the degradation of a surrogate compound, benzoate, in the presence of GDD under ambient sunlight. In typical urban atmospheres (high NO_x levels) with relative humidity higher than 40%, authentic dust can be easily nitrated, elevating dust's hygroscopicity and significantly increasing SOA growth potential.

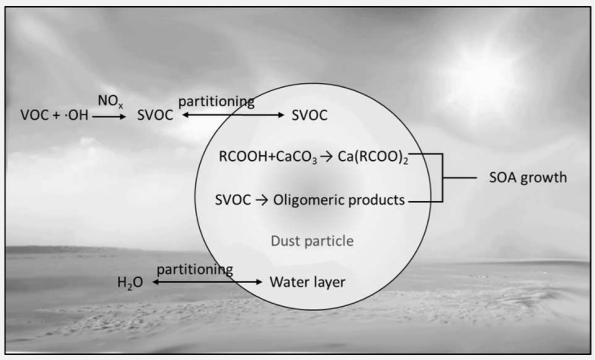

KEYWORDS: *heterogeneous reaction, secondary organic aerosol, gasoline, Gobi Desert dust, hygroscopicity, aromatic SOA*

Downloaded via UNIV OF FLORIDA on July 8, 2020 at 22:54:55 (UTC).
See https://pubs.acs.org/sharingguidelines for options on how to legitimately share published articles.

1. INTRODUCTION

Mineral dust from desert and semidesert regions is frequently introduced into the atmosphere by strong wind and is known as the most abundant aerosol in the atmosphere, ranging from 1000 to 3000 Tg annually.[1,2] These dust particles undergo long-range transport, that is, from Central Asia to Western North America.[3] When dust plumes pass through polluted urban regions, the dust particles provide surfaces to uptake trace gases, such as SO_2, NO_x, ozone, and volatile organic compounds (VOCs).

Most studies have focused on the heterogeneous uptake of inorganic trace gases on dust particles,[4−11] and few studies have attempted to investigate the uptake of VOCs on mineral dust particles.[12−19] Some VOCs can undergo photooxidation in the atmosphere and produce semi-VOCs (SVOCs). SVOCs play an important role in secondary organic aerosol (SOA) formation, which is a major contributor to the organic carbon budget on a global scale[20−23] and in the urban atmosphere.[24] To date, the impact of authentic dust particles on SOA growth has been poorly studied. Several field studies[25,26] reported a significant increase of carboxylic acids during the dust event (spring of 2009, 2011, and 2013) in the urban center of Xi'an, China. The long-range transport of the Asian alkaline dust carried with carboxylic acids was also observed by Mochizuki et al.[27] at the Murodo-Daira snowfield, Japan, in 2009 and 2001. However, the mechanistic role of the mineral dust in SOA growth is uncertain under typical polluted urban environments.

Unlike pure metal oxides, authentic mineral dust particles contain a variety of metal oxides and inorganic salts.[28] The semiconducting metal oxides (i.e., TiO_2 and Fe_2O_3) in dust particles are able to photochemically generate OH radicals[10] and further influence on heterogeneous reactions of organic species and modulate SOA growth. The inorganic salts in authentic dust particles, that is, calcium nitrate, are hygroscopic and can absorb water on dust under the ambient conditions with relative humidity (RH) ranging from 15 to 80%.[29−32] Numerous studies reported the enhancement of the SOA mass in the presence of aerosol water content because of the promotion of heterogeneous reactions of reactive oxygenated products.[33−36] Therefore, with adequate water content in

Received: July 11, 2019
Revised: August 30, 2019
Accepted: September 3, 2019
Published: September 3, 2019

ACS Publications © 2019 American Chemical Society

DOI: 10.1021/acsearthspacechem.9b00195
ACS Earth Space Chem. 2019, 3, 2404−2414

Table 1. Outdoor Chamber Experimental Conditions for SOA Formation and SOA Growth

no.	date[a]	VOC[b]	seed type[c]	seed mass (μg m^{-3})[d]	VOC initial (ppbC)[d]	NO/NO$_2$ (ppb/ppb)[d]	VOC/NO$_x$ (ppbC ppb^{-1})	Temp. (K)[d]	RH (%)[d]	comments
1	03/02/18-E	toluene	dGDD	898	1386	130[e]	10.7	297.4−311.5	21−39	Figures 1, 3, and 4
2	03/02/18-W	toluene	no seed	N.A.[f]	1449	128[e]	11.3	293.9−310.4	26−40	Figures 1, 3, and 4
3	02/25/19-E	gasoline	no seed	N.A.[f]	1862	86/123	8.9	290.4−305.3	15−32	Figures 1, 3, and 4
4	02/25/19-W	gasoline	dGDD	402	1883	75/139	8.8	287.7−305.6	18−41	Figures 1, 3, and 4
5	06/16/19-E	TMB	dGDD	376	1701	66/116	9.4	308.7−319.7	14−32	Figures 1, 3, and 4
6	06/16/19-W	TMB	no seed	N.A.[f]	1638	62/122	8.9	305.7−319.4	22−35	Figures 1, 3, and 4
7	06/24/19-E	TMB	dSilica	209	1647	66/116	9.1	309.1−320.5	13−28	Figures 1, 3, and 4
8	06/24/19-W	TMB	no seed	N.A.[f]	1746	62/122	9.5	305.9−317.2	22−31	Figures 1, 3, and 4
9	06/14/19-E	TMB	dGDD	409	1647	76/108	8.9	310.8−318.8	15−23	Figure 6
10	06/14/19-W	TMB	wGDD	434	1593	73/107	8.8	307.5−316.5	49−71	Figure 6
11	09/13/18-E	TMB	dAS	39	801	35/67	8.0	310.9−325.1	11−21	Figure 6
12	09/13/18-W	TMB	dGDD	452	855	30/68	8.9	307.6−322.8	18−31	Figure 6
13	11/17/18-E	TMB	wGDD	496	918	26/67	10.0	283.9−307.3	40−66	Figure 6
14	11/17/18-W	TMB	wAS	242	909	24/69	9.9	281.9−307.0	47−78	Figure 6

[a]"E" and "W" denote the east and west sides of the outdoor chamber. [b]"VOCs" represent volatile organic compounds. "TMB" represents 1,3,5-trimethylbenzene. [c]"dGDD" and "wGDD" denote GDD particles under the dry (RH < 40%) and the wet (RH > 40%) experimental conditions, respectively. "dAS" and "wAS" denote AS seeds under the dry (RH < ERH < 40%) and the wet conditions (RH > ERH > 40%), respectively. "dSilica" represents the silica particles under the dry conditions (RH < 40%). [d]The errors associated with the concentration of VOCs, NO$_x$, and seed mass were ±10, ±6.5, and ±6%, respectively, according to the measurement uncertainty. The errors of temperature (Temp.) and RH were ±0.5 K and ±5%, respectively. [e]Gaseous nitrous acid (HONO) was used for Exps. 1 and 2 to accelerate the photooxidation of toluene. HOHO was generated by the reaction of 0.1 M $NaNO_2$ and 1 M H_2SO_4 using a three-way flask with clean air passing through. The concentration of HONO was estimated by the difference of NO$_x$ concentration with and without a base denuder (coated with 1% Na_2CO_3 and 1% sugar).[43] [f]N.A.: not applicable.

authentic mineral dust particles, the impact of dust hygroscopicity on SOA growth needs to be investigated.

In the current work, we explore the impact of dust particles [Gobi Desert dust (GDD) particles] on the photooxidation of three VOC precursors (toluene, 1,3,5-trimethylbenzene (TMB), and gasoline vapor) in the presence of NO$_x$ using an outdoor chamber. Aromatic hydrocarbons (HCs) and gasoline were chosen to mimic the urban environments. The changes in aerosol composition due to the atmospheric processes were also characterized using Fourier transform infrared spectroscopy (FTIR) and a particle-into-liquid sampler combined with ion chromatography (PILS-IC). Benzoic acid and sodium benzoate-coated GDD samples were chosen as the surrogate compounds to investigate the heterogeneous photocatalytic oxidation of organic products on GDD surfaces. The photodegradation of benzoate in the benzoate-coated GDD samples under sunlight was measured using gas chromatography−mass spectrometry (GC−MS). To understand the role of dust hygroscopicity in SOA growth, TMB was photooxidized in the presence of GDD particles under the dry (RH: 20−40%) or the wet conditions (RH: 40−80%). In addition, the environmental implications of these results are discussed.

2. MATERIALS AND METHODS

2.1. Dust Samples and Chemicals. The GDD particles used in this study were collected from the surface of desert in Tsogt-Ovoo soum in the Ömnogövi Province, Mongolia, between March and May 2015. The collected dust samples were sieved to less than 20 μm. The elemental fractions of these GDD samples were previously reported by Park et al.[28] (also see Figure S1). The Brunauer−Emmett−Teller (BET) surface area of GDD particles is estimated to be 40 ± 2 m^2 g^{-1}. The buffering capacity of GDD particles is the capacity to buffer acid, which was estimated to be 3.2×10^{-4} μmol per μg by Yu and Jang.[31] For outdoor chamber experiments, amorphous silica particles and aerosolized ammonium sulfate (AS) particles were used. The silica particles (NanoCym Inc., USA) are polydisperse particles with a mean diameter of 500 nm and a BET surface area of 5.9 ± 0.3 m^2 g^{-1}. The AS seeds were directly aerosolized from AS solution (0.05 mol L^{-1}) using a constant output atomizer. Three types of SOA precursors, TMB (Sigma-Aldrich, 98%), toluene (ACROS, 99.5%), and gasoline vapor (#93, purchased from BP. Inc. at Gainesville, Florida on May 3, 2018), were used. The gasoline has an average density of 0.75 g mL^{-1} and an average molecular weight of 114 g mol^{-1}. The composition of gasoline vapor was estimated using a GC-flame ionization detector (GC-FID; HP 5890) as shown in Table S1. For the outdoor chamber experiments, NO$_x$ (NO/NO$_2$ ≈ 0.5) was directly injected into the chamber. NO$_2$ was used to accelerate the formation of nitric acid. To study the photooxidation of organic products on dust, GDD particles were coated by the surrogate organic compounds, benzoic acid (Sigma-Aldrich; ≥99.5%) or sodium benzoate (Sigma-Aldrich; ≥99%). The organic compound-coated GDD samples were then exposed to sunlight in the ambient conditions. The detailed preparation of the pre-coated GDD samples is described in Section S1.

2.2. Outdoor Chamber Experiments. SOA was produced from three different types of precursors (TMB,

DOI: 10.1021/acsearthspacechem.9b00195
ACS Earth Space Chem. 2019, 3, 2404−2414

toluene, and gasoline vapor) using the Atmospheric PHotochemical Outdoor Reactor (UF-APHOR) dual chamber (52 m^3 each) located at the University of Florida. The operation of the large outdoor smog chamber has been described previously[31,37−39] (also see Section S2). VOCs were evaporated into the chamber by a syringe with heating. Nonreactive CCl_4 (400 ppb) was used as the chamber dilution indicator. The concentration of the gas-phase VOC was monitored by GC-FID. The concentrations of ozone and NO_x were measured by a photometric ozone analyzer (model 400E, Teledyne) and a chemiluminescence NO/NO_x analyzer (model T201, Teledyne), respectively. The inorganic ion concentrations were measured using a PILS-IC (Applikon, ADISO 2081; Compact IC 761, Metrohm). The particle size distribution was monitored by the combination of a SMPS (SMPS 3080, TSI) and an optical particle sizer (OPS 330, TSI) via the Multi-Instrument Manager software (MIM2, TSI). The organic carbon concentration was monitored using an organic carbon/elemental carbon aerosol analyzer (OC/EC model 4, Sunset Laboratory Inc.) for every 50 min. The concentration of organic matter (OM, $\mu g\ m^{-3}$) was calculated based on OC concentration and an OM to OC ratio. The averaged OM to OC ratios of SOA generated from toluene, TMB, and gasoline vapor are assumed to be 1.7, 1.9, and 1.6, respectively.[40−42] The OM concentration was corrected by the particle loss to the chamber wall using a particle loss factor. The loss factor was measured for each size bin using AS seeds and fresh GDD particles. The SOA yield was then calculated as the maximum OM concentration divided by the consumption of VOCs. The consumption of gasoline was estimated based on the reaction rate constants of aromatic VOCs with OH radicals in the gas phase (Table S1) and the measured toluene concentration during the experiments (Figure S2). The meteorological variables, that is, temperature, RH, sunlight intensity, and sunlight spectrum, were monitored on both inside and outside the chamber using a hygrometer (CR1000 Measurement and Control System, Campbell Scientific), a fibro-optical portable spectrometer (EPP2000, Stellar Net Inc., USA), and an ultraviolet radiometer (TUVR, Eppley Laboratory Inc.), respectively. The details of the outdoor chamber experiments are summarized in Table 1. The consumption of VOCs (Figure S2), the concentration of ozone and NO_x (Figure S3), and the time profiles of environmental variables (Figure S4) can be found in the Supporting Information. An example of particle size distributions for aerosols with and without GDD particles is shown in Figure S5. For both GDD-seeded and SiO_2-seeded experiments, the formation of new particles was not observed, suggesting that the condensation of organic products on the preexisting seeds led to SOA growth.

For the toluene and gasoline experiments (Exps. 1−4 in Table 1), the SOA composition was measured using FTIR (Nicolet Magma 560, Madison, WI, USA). SOA-coated GDD was collected by impacting a silicon FTIR window (13 × 2 mm, Sigma-Aldrich, St Louis, MO, USA). The samples were collected for a duration of 120 min started at 12 pm of each experiment. After the sampling, the collected samples were immediately analyzed using FTIR by recording the spectra from 800 to 4000 cm^{-1} with purging of dry clean air at RH < 5%. The mass of silicon FTIR window was measured using an analytical balance before and after the impaction. The samples were measured for three data points by rotation of the silicon window and averaged. The detailed peak assignments for the functional groups are described in Table S2.

2.3. Characterization of Photooxidation of Organic Compounds in Dust Particles. To test the photocatalytic degradation of organic compounds on dust, benzoic acid and sodium benzoate were chosen as surrogate compounds. The benzoic acid-coated GDD particle (GDD-BZA) and sodium benzoate-coated GDD particle (GDD-sodium benzoate) were exposed to sunlight for 2, 4, 6, and 8 h in the open-air environment. The pretreatment of these samples is illustrated in Section S1 in the Supporting Information. After the experiments, the samples were extracted by acetone (Fisher Chemical; ≥99.5%) and then derived using pentafluorobenzyl bromide (PFBBr, Sigma-Aldrich ≥99%) and measured using GC−MS (Varian 3800/2000 GC/MS, Palo Alto, USA) in the electron impact (EI) mode. For control, pure sodium benzoate (Sigma-Aldrich; ≥99%) was tested with the same procedure. The photocatalytic experiments were performed in three duplicates. The details of the PFBBr derivation procedure were reported in the previous studies.[44,45] In brief, 10 μL of PFBBr reagent (34.56 $\mu g\ \mu L^{-1}$ in acetonitrile) and 10 mg of potassium carbonate powder were added to the sample vials. The samples were then kept at 50 °C for 24 h before analysis. Ten microliters of internal standard (0.0237 $\mu g\ \mu L^{-1}$ d_6-naphthalene, 0.027 $\mu g\ \mu L^{-1}$ d_{10}-anthracene in toluene, 1.836 $\mu g\ \mu L^{-1}$ heptanoic acid in acetonitrile) and 10 μL of recovery standard (0.012 $\mu g\ \mu L^{-1}$ decafluorobiphenyl in methylene dichloride) were added to the sample vials before analysis. An averaged recovery higher than 80% was observed. For quantification, an external calibration was conducted for benzoic acid and sodium benzoate using GC−MS under the same procedure.

2.4. Dust Water Content. The aerosol water content plays an import role in the formation of SOA because the partitioning of the polar SOA products increases with increasing liquid water content and further enhances the aqueous-phase reactions.[36,46,47] Thermodynamic models, such as E-AIM II[48−50] and ISORROPIA,[51,52] provide a solution to the prediction of the aqueous-phase water content (i.e., AS aerosol) but may not be applicable for the dust particles because of the complexity in heterogeneous reactions. GDD particles, which consist of metal oxides and inorganic salts, are usually coated with a multilayer of water under the typical ambient RH ranging from 20 to 80%.[30,31,53] Gobi dust particles are enriched in carbonates (i.e., calcite), which are able to buffer the acidic trace gases and lead to hygroscopic salts (i.e., calcium nitrate and sodium nitrate). These hydrophilic salts in dust particles can be hydrated at the relative low RH environment.[54−56] It has been previously reported by Yu and Jang[31] that the hygroscopicity of dust particles is greatly modified by the photochemical aging in the presence of NO_x. The water content in GDD particles can be estimated by a semiempirical additive equation as follows

$$F_{water} = 0.03(e^{3.6\cdot RH} - 1) + 1.4\, e^{4.0\cdot RH}[NO_3^-]_{dust} \quad (1)$$

where F_{water} ($\mu g\ \mu g^{-1}$) is the water mass normalized by dry dust mass, RH is the relative humidity (0.2−0.8), and $[NO_3^-]_{dust}$ is the concentration of nitrate ($\mu g\ \mu g^{-1}$) in the dust. The value of $[NO_3^-]_{dust}$ is limited to the reactive carbonate content on the surface of dust particles. The impact of the organic coating on dust hygroscopicity is not considered in eq 1.

DOI: 10.1021/acsearthspacechem.9b00195
ACS Earth Space Chem. 2019, 3, 2404−2414

3. RESULTS AND DISCUSSION

3.1. Formation of SOA in the Presence of Airborne GDD Particles. To understand the role of mineral dust in SOA growth, three VOC precursors (toluene, TMB, and gasoline vapor) were photooxidized in the presence of NO_x and GDD particles under dry conditions (RH < 40%) using the outdoor smog chamber. Figure 1 compares the maximum SOA yields in the presence and absence of mineral particles. The time profiles of OM concentrations are shown in Figure S6.

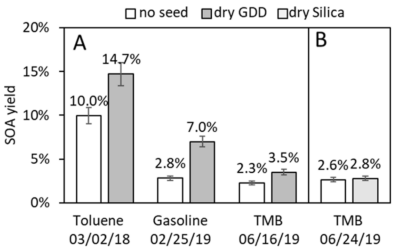

Figure 1. Yields of SOA formed from three different precursors under the dry conditions (RH < 40%): toluene (03/02/2018), gasoline (02/25/2019), TMB (06/16/2019), and TMB (06/24/2019). The experiments were conducted in (A) with and without GDD particles and (B) with and without dry silica particles. The errors associated with the SOA yield were estimated from the uncertainties of organic mass and the consumption of precursors by the propagation of the uncertainty. The results were corrected for the particle loss to the chamber wall as described in Section 2.2. The time profile of the OM concentration is shown in Figure S6.

As seen in Figure 1A, the SOA yields in the presence of GDD particles are significantly higher than that in the absence of GDD particles. Under this circumstance, gas-particle partitioning of oxygenated products on dust particles is processed in the absorption mode (multilayer of water molecular on GDD particles), and the impact of the surface area of dust particles on SOA growth is insignificant. The similar tendency was also reported in SOA growth in the presence of the dry AS seed aerosol.[57,58] To investigate the influence of surface area on SOA formation and growth, the SOA yield of TMB in the presence of silica particles was compared with that without seeds. Evidently, no difference in SOA yields appears between TMB SOA with silica particles and that without silica particles (Figure 1B).

In addition, the authentic mineral dust particles, such as GDD, contain a variety of metal oxides and inorganic salts.[28] Specifically, semiconductive metal oxides in dust particles can photocatalytically oxidize organic products on dust particles. Hygroscopic inorganic slats absorb water vapor and promote heterogeneous reactions of reactive oxygenated products, such as aldehydes, to form oligomeric products.[33−35] For heterogeneous chemistry of organic products on dust particles, we propose three reaction mechanisms: (1) the formation of carboxylate salts by the reaction of alkaline carbonates with carboxylic acids (Section 3.2);[15,59,60] (2) the photooxidation of the SVOC products partitioned on dust particles, leading to both highly oxidized multifunctional (HOM) compounds and intermediate VOCs (IVOCs) (Section 3.3);[12,61] and (3) heterogeneous reactions of oxygenated products in dust-phase water layers (Section 3.5).[33−35] Figure 2 summarizes the mechanistic role of mineral dust in SOA growth.

3.2. Formation of Nitrate and Carboxylates on Dust Particles. Nitric acid is known to quickly form on dust surfaces or through the photochemical reaction of NO_x in the gas phase.[62,63] As shown in Figure 3, the mass fraction of nitrate on dust particles rapidly increases in the morning. It has been previously reported that high water contents on dust particles enhance the uptake of NO_x.[10,64] Typically, RH is high in the morning and nitric acid formation is rapid immediately after sunrise. As alkaline carbonates (i.e., $CaCO_3$ and Na_2CO_3) are the major constituents in authentic mineral dust particles,[65−67] these carbonates can quickly react with nitric acid on GDD particles to form nitrate salts as follows.

$$CaCO_3 + 2HNO_3 \rightarrow Ca(NO_3)_2 + H_2O + CO_2\uparrow \quad (2)$$

For all the experiments in Figure 3, nitrates reach to the maximum concentrations after 3 h from the beginning of the experiments and are gradually depleted. It has been previously reported by Wang and Laskin[68] that the nitrate in calcium

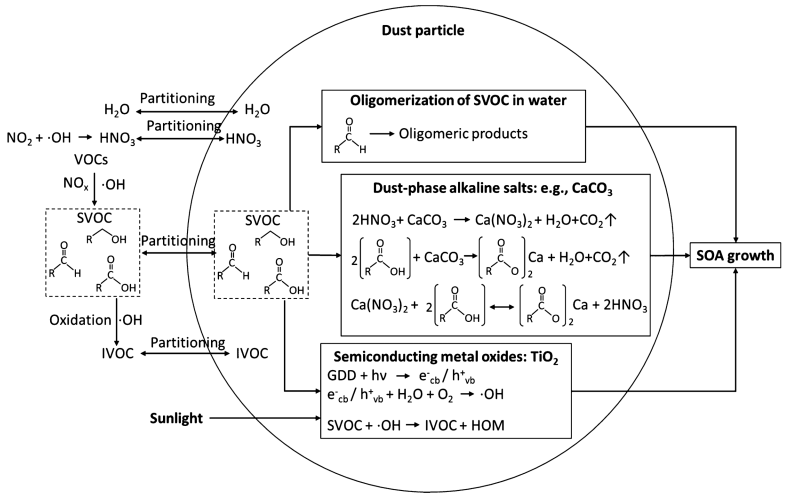

Figure 2. Reaction mechanisms for the heterogeneous formation of oxygenated organic products on the surface of GDD particles in the presence of NO_x under sunlight. "SVOC", "IVOC", and "HOM" represent SVOC, IVOC, and HOM compound, respectively. The volatility of SVOC is assumed to be higher than that of the HOM compound but lower than that of IVOC.

DOI: 10.1021/acsearthspacechem.9b00195
ACS Earth Space Chem. 2019, 3, 2404−2414

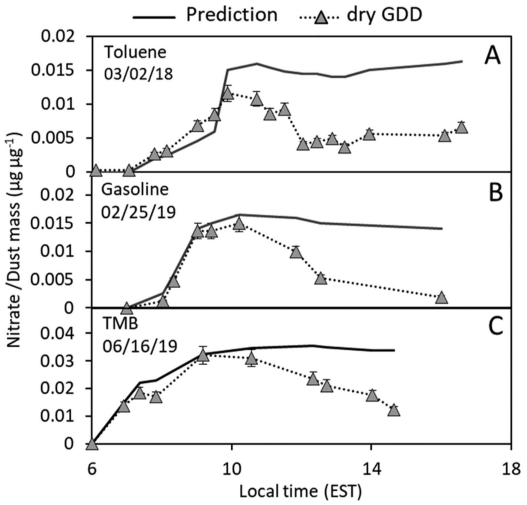

Figure 3. Time profiles of observed nitrate concentration in the presence of dry GDD particles for (A) toluene (03/02/18), (B) gasoline vapor (02/25/19), and (C) TMB (06/16/19). The errors associated with nitrate concentration were estimated from the uncertainty of measurement. The solid line represents the concentration of nitrate that was predicted using the AMAR model.

nitrate can react with the water-soluble organic acid and release gaseous nitric acid. The formed nitrate salts in dust particles as described in eq 2 (i.e., $Ca(NO_3)_2$ and $NaNO_3$) can experience acid displacement that nitrate is substituted by the relatively less volatile organic acid driven by the evaporation of nitric acid.

$$Ca(NO_3)_2 + 2RC(O)OH \leftrightharpoons Ca(RC(O)O)_2 + 2HNO_3 \quad (3)$$

The formation of nitrate salts and carboxylates is limited to the buffering capacity of GDD particles (3.2×10^{-4} μmol μg^{-1}).[31] Thus, nitric acid competes with carboxylic acid to react with the limited amount of carbonates on dust surfaces. Under the dry conditions, nitrates on dust surfaces are gradually depleted by carboxylic acids produced during photochemical reactions of VOCs.

It is to be noted that the partitioned nitric acid on dust is impacted by the dust-phase water content because of its high water solubility (the Henry's law constant of nitrate acid > 10^3 mol m^{-3} Pa^{-1}).[48] To study the depletion of nitrate on dust particles, three chamber experiments in Figure 3 were simulated for the nitrate concentration using the Atmospheric Mineral Aerosol Reaction (AMAR) model.[31] The AMAR model was recently derived to capture the heterogeneous formation of sulfate and nitrate in the presence of mineral dust particles. To simulate the photooxidation of VOCs in the gas phase, the carbon bond mechanism (CB6)[69] was employed. In this study, the AMAR model was performed using a chemistry box model platform, the Dynamically Simple Model for Atmospheric Chemical Complexity (DSMACC).[70] As shown in Figure 3, the gap of the nitrate concentration between model prediction and observation is attributed to the nitrate depletion by forming carboxylates because the AMAR model is incapable of processing heterogeneous reactions of organic compounds on dust particles.

Figure 4 shows FTIR spectra (800−4000 cm^{-1}) of SOA formed from the photooxidation of toluene or gasoline vapor in the presence of GDD particles. The FTIR data also support the depletion of carbonate and nitrate from GDD particles by forming carboxylate salts. As seen in the FTIR spectrum of fresh GDD particles (Figure S7A), the carbonate peak appears at 1450 cm^{-1} and the Si−O−Si peak of GDD particles at 1040 cm^{-1}. Figure S7B shows the FTIR spectrum of pure calcium nitrate (tetrahydrate): nitrate peak at 1380 cm^{-1}. For all the spectra in Figure 4, the water content in particles is very little (negligible) because the FTIR spectra were measured under the dry condition by purging the spectrometer with the dry tank air (RH < 5%). Figure 4A,B shows the spectra of toluene SOA solely and toluene-SOA-coated GDD particles, respectively. In Figure 4A, a strong and broad O−H stretching

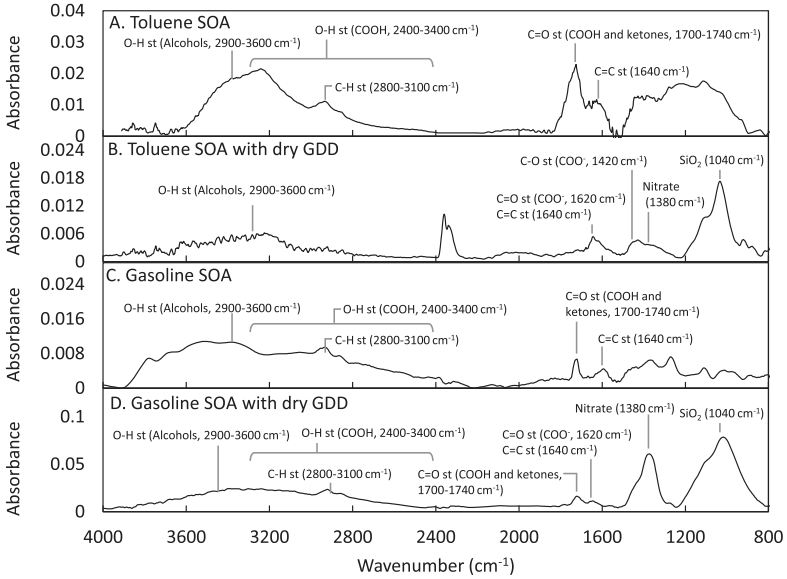

Figure 4. FTIR spectra (800−4000 cm^{-1}) of (A) toluene SOA (03/02/18), (B) toluene-SOA coated on dry GDD particles (03/02/18), (C) gasoline SOA (02/25/19), and (D) gasoline-SOA coated on dry GDD particles (02/25/19). The spectra were averaged for three measurements. The peak assignments of functional groups are listed in Table S2.

DOI: 10.1021/acsearthspacechem.9b00195
ACS Earth Space Chem. 2019, 3, 2404−2414

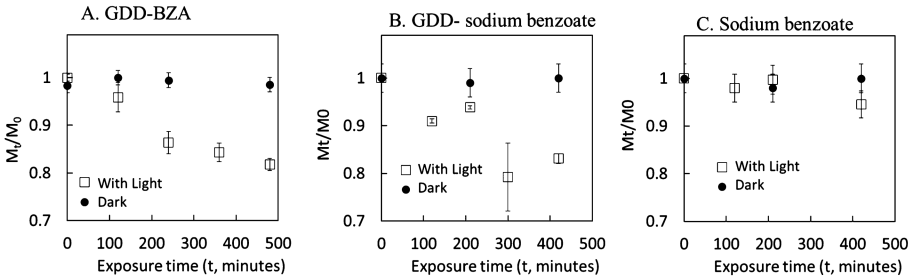

Figure 5. Time profiles of the benzoate concentration (M_t) normalized by initial concentration (M_0) on (A) GDD-BZA under sunlight (from 9 am to 5 pm on Dec 5, 2018) and dark; (B) GDD-sodium benzoate under sunlight (from 9 am to 5 pm on Dec 12, 2018) and dark; and (C) pure sodium benzoate under sunlight (from 9 am to 5 pm on Dec 12, 2018). The amount of benzoic acid or benzoate in (A−C) is similar (20−30 μg per sample). The errors were obtained from the standard deviation of three replicates.

associated with alcohol appears between 2900 and 3600 cm^{-1}. The broad O−H stretching of carboxylic acid in toluene SOA ranges between 2400 and 3400 cm^{-1}. The peaks between 2800 and 3100 cm^{-1} are from C−H stretching. Carbonyl bond stretching (carboxylic acid and ketone) appears between 1700 and 1740 cm^{-1}. In general, carbonyls from multifunctional aldehydes, which are reactive and polymerized in the aerosol phase, would be little in SOA. The FTIR stretching of the conjugated alkenes, which originate from the aromatic ring-opening reactions, is seen at 1640 cm^{-1}. However, the FTIR spectrum (Figure 4B) of toluene-SOA-coated GDD is very different from the FTIR spectrum of toluene SOA (Figure 4A). As seen in PILS-IC data (Figure 3A), carbonate in dust was quickly depleted by nitrate in the early morning and nitrate was further depleted by organic carboxylic acid. Evidently, Figure 4B shows a typical carboxylate pattern with peaks at 1620 cm^{-1} (C═O stretching) and 1420 cm^{-1} (C−O stretching). The peak at 1420 cm^{-1} should not originate from carbonate, which was depleted by nitrate (Figure 3A). Figure 4B shows no clear carbonyl peak between 1700 and 1740 cm^{-1}, which is observed in Figure 4A, suggesting that the carbonyl in Figure 4B is in the form of carboxylate at 1620 cm^{-1}. A similar tendency with toluene SOA (Figure 4A) and toluene-SOA coated GDD (Figure 4B) can be found in gasoline SOA (Figure 4C) and gasoline-SOA-coated GDD (Figure 4D). Unlike the spectrum of toluene-SOA-coated GDD (Figure 4B), the spectrum of gasoline-SOA-coated GDD shows a higher nitrate peak at 1380 cm^{-1} because of the difference in the aerosol aging stage during the sampling and the different reaction rates of carboxylic acids with alkaline inorganic salts (Figure 3B). We conclude that the composition of SOA on dust particles is very different from that of SOA without preexisting seeds. In addition, the surface property of dust particles can be significantly modified during the aging process in the presence of NO_x and VOC.

3.3. Photooxidation of Organic Species on Dust Particles. Dust particles interact with organic products via heterogeneous photocatalytic reactions. The semiconducting metal oxides (i.e., TiO_2 and Fe_2O_3) in dust particles can be photoactive when receiving photons (i.e., sunlight) and generate electron and hole pairs (e_{cb}^-/h_{vb}^+)[71,72] that further react with water or oxygen molecules to form OH radicals. To study the photooxidation of organic products on dust, the surrogate organic compounds, benzoic acid and sodium benzoate, were coated on GDD particles and irradiated under sunlight. Figure 5 shows the change of the concentration of benzoate in three different samples: GDD-BZA, GDD-sodium benzoate, and pure sodium benzoate. Figure 5A,B clearly shows the decay of benzoate as a function of time in both GDD-BZA and GDD-sodium benzoate samples. The sodium benzoate in Figure 5C was used as a control for the observation in Figure 5B. The reduction of benzoate in the pure sodium benzoate samples is insignificant within errors. The benzoate in the presence of GDD particles was decomposed to form probably less volatile IVOC and further off-gassing from the dust surface. The electrons and holes can also directly react with the absorbed organic compounds, but this reaction is minor because of the significant amount of water or oxygen molecules compared to the organic products. Previous laboratory studies showed that the dust-generated surface radicals could oxidize trace gases, such as SO_2 and NO_x, through heterogeneous oxidation reactions.[32,73] In addition, the formation of dust-driven oxidants, that is, OH radicals, can be promoted at the higher RH[31] and further oxidize SOA products.

It has been reported that trace gases, such as SO_2, are autoxidized on the dust surface in oxygen environments.[6,10,74] However, heterogeneous photooxidation is dominant under ambient sunlight over the autoxidation of trace gases. To ensure that the degradation of organic compounds is promoted by the heterogenous photooxidation mechanism, both GDD-BZA and GDD-sodium benzoate stood for 8 h under dark, shown as the filled symbols in Figure 5A,B. The reduction of benzoate was negligible in both experiments. Hence, we conclude that dust particles can heterogeneously oxidize organic species when dust photoactivation is active. Similar results were also found by Chen et al.[75] in which the SOA growth originated from *m*-xylene was suppressed in the presence of TiO_2 particles under UV light because of the photooxidation of oxygenated products on TiO_2 particles. Alternatively, the SVOC products on dust can be oxidized by OH radicals to form less volatile HOM compounds, resulting in an increase of SOA yield. For example, the oxidation state (O to C ratio) of α-pinene SOA in the presence of TiO_2 particles was reported to be increased under UV irradiation,[61] which verified the oxidation of organic compounds on the dust surface. Therefore, the effects of photocatalytic oxidation of SVOC on the SOA yield are probably compensated by the formation of both less volatile HOM compounds and more volatile IVOCs.

In addition to the photoactivation of dust, dust-phase OH radicals can form via the heterogeneous reaction of O_3 and NO_2. Ozone is heterogeneously decayed on dust surfaces to form an atomic oxygen and an oxygen molecule.[76,77] This atomic oxygen bonded on dust surfaces can yield a OH radical by reaction with a water molecule and therefore accelerate

DOI: 10.1021/acsearthspacechem.9b00195
ACS Earth Space Chem. 2019, 3, 2404−2414

heterogeneous oxidation of organic species on dust. NO_2 is also found to heterogeneously convert to HONO on the dust surface both in the dark[78] and under UV light.[79] HONO can further photolysis and generate OH radicals. Therefore, the concentration of OH radicals on dust particles can be impacted by the concentration of ozone and NO_x and further impact the heterogeneous reactions.

3.4. Characteristic Time of Dust-Driven Photocatalytic Oxidation and Gas-Phase Photooxidation of SVOC. In order to investigate the impact of dust particles on the atmospheric pathway of organic products, the characteristic time ($\tau_{dust,OH}$, s) of heterogenous photocatalytic oxidation of SVOC was compared to that of the gas-phase oxidation of SVOC with a OH radical ($\tau_{gas,OH}$, s). As discussed in Section 3.3, SVOC products partitioned on dust particles can be further oxidized by forming less volatile HOM compounds as well as more volatile IVOCs (oxidation with carbon−carbon bond breakage). This reaction can be described as follows

$$\mathrm{SVOC}_i + \bullet\mathrm{OH(dust)} \rightarrow \alpha_1\mathrm{HOM}_1 + \ldots + \beta_1\mathrm{IVOC}_1 \ldots + \mathrm{CO_2} + \mathrm{H_2O} \qquad k_{\mathrm{dust\_OH},\,i} \tag{4}$$

where $k_{dust\_OH,i}$ (cm^3 $molecular^{-1}$ s^{-1}) is the reaction rate constant of $SVOC_i$ with a OH radical on dust particles. $\tau_{dust,OH}$ is then estimated by

$$\tau_{\mathrm{dust,OH}} = \frac{1 + K_{\mathrm{dust},i}\cdot M_{\mathrm{water}}}{k_{\mathrm{dust\_OH},i}\cdot C_{\mathrm{OH,dust}}\cdot K_{\mathrm{p},i}\cdot M_{\mathrm{water}}} \tag{5}$$

where $K_{dust,i}$ (m^3 μg^{-1}) is the gas-dust partitioning constant of $SVOC_i$ and M_{water} (μg m^{-3}) is the concentration of water content in dust particles. The detailed derivation of $\tau_{dust,OH}$ can be found in Section S4. The concentration of dust-phase OH radicals ($C_{OH,dust}$) is influenced by RH, sunlight intensity, and the absorbed chemical species (i.e., ozone and NO_x) on dust particles. $\tau_{dust,OH}$ increases as $k_{dust\_OH,i}$ or $C_{OH,dust}$ increases. $C_{OH,dust}$ and $k_{dust\_OH,i}$ were predicted using the AMAR model under the three RHs (20, 50, and 80%) at a given sunlight intensity (at 12 pm on 03/02/2018, Exp. 1 in Table 1 and Figure S8). Figure S9 illustrates $\tau_{dust,OH}$ of two SVOCs (two different vapor pressures (P_L, mm Hg) = 10^{-3} and 10^{-5} mm Hg). The variation of $\tau_{dust,OH}$ is large ranging from 1 h to several weeks (1 to 10^3 h) under varying P_L, RH, and M_{water}. For example, $\tau_{dust,OH}$ (1−40 h) at 80% RH is 1 order of magnitude smaller than that at 20% RH. For the estimation of $\tau_{gas,OH}$ (s), the concentration of OH radicals is set to 10^6 molecules cm^{-3} (at typical polluted urban areas), and the reaction rate constant of SVOC with OH radicals is set to 10^{-11} cm^3 $molecules^{-1}$ s^{-1} (i.e., $k_{OH,toluene} = 5.63 \times 10^{-12}$ cm^3 $molecules^{-1}$ s^{-1}). Unlike $\tau_{dust,OH}$, $\tau_{gas,OH}$ is insensitive to RH (Figure S9). $\tau_{dust,OH}$ (<5 h) of the SVOC with $P_L = 10^{-5}$ mm Hg at RH = 80% is much shorter than $\tau_{gas,OH}$ (28 h). At RH = 20%, $\tau_{dust,OH}$ (>200 h) of SVOC with $P_L = 10^{-3}$ mm Hg is longer than the reported lifetime of airborne dust particles (approximately 100 h).[3,80,81] The contribution of SVOC with $P_L \leq 10^{-3}$ mm Hg to total organic carbons (gas + particle) varies from 15 to 40% under varying NO_x conditions and atmospheric HC processes.[36] Hence, a significant fraction of oxygenated products can be affected by air-suspended dust particles in the ambient RH.

3.5. Impact of Dust Hygroscopicity on SOA Growth. As discussed in Section 3.1, SOA can be formed via the aqueous reaction of oxygenated products in dust particles to form oligomeric products. Figure 6 illustrates the impact of dust hygroscopicity on TMB SOA growth. As shown in Figure 6A, the SOA yield with wet GDD particles (averaged RH = 57.6%) is ~2.5 times higher than that with dry GDD (averaged RH = 18.8%). The water content of authentic dust particles follows an exponential manner as RH increases without showing the clear phase transition.[28] Therefore, heterogeneous reaction of oxygenated organic products is enhanced in wet GDD particles. Unlike GDD, AS aerosol is solid at the RH lower than its efflorescent RH. Under the dry conditions (Figure 6B), the water content in both AS and GDD particles is nearly negligible. However, the enhancement in the SOA yield appeared in the presence of dry GDD compared to that with dry AS. As discussed in Section 3.2, SOA growth can be enhanced by the formation of carboxylate salts in dust particles. As seen in Figure 6C, no apparent difference in SOA yields was observed between the SOA with wet GDD and that with wet AS. This can also be supported by the predicted water content as shown in Figure S9 where both wet GDD and wet AS seeds contain a significant amount of aerosol phase water. For the formation of SOA in the presence of wet dust particles, the pathway via heterogeneous reactions of oxygenated products is more important than the pathway via the formation of carboxylate salts. Therefore, dust's buffering capacity limits the formation of carboxylate salts in the dry condition and the quantity of reactive organic compounds limits SOA growth in the wet condition.

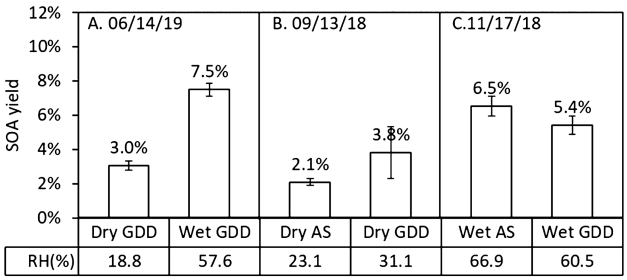

Figure 6. Comparison of SOA yields formed from TMB in the presence of (A) dry GDD and wet GDD particles (06/14/19), (B) dry GDD and dry AS particles (09/13/18), and (C) wet AS and wet GDD particles (11/17/18). The averaged RH (%) is also listed for each experiment. The SOA yield was corrected by the particle loss to the chamber wall. The errors were estimated by the propagation errors from yield calculation.

Figure S11 displays the time profile of nitrate on dust particles in all three experiments (Figure 6). The depletion of nitrate appeared only with dry GDD. However, hydrophilic HNO_3 vapor considerably partitions to wet GDD and exceeds GDD's buffering capacity. This abundant nitric acid (acid dissociation constant, $pK_a = -1.37$)[82] built on GDD particles suppresses gas-dust partitioning of weakly acidic carboxylic acid (pK_a ranges from 1 to 4).[82] As described in eqs 2 and 3, nitric acid competes with carboxylic acids for the reactions with alkaline carbonate, that is, $CaCO_3$. Figure S11B,D clearly evinces the absence of carboxylate salts (no depletion of nitrate) in the presence of wet GDD. Figure S12 illustrates that the salt (benzoate) of an intermediate volatile carboxylic acid (benzoic acid) can be depleted by nitric acid that is generated from the photochemical reaction of NO_2. This result confirms that in the presence of wet GDD gas-dust partitioning of

DOI: 10.1021/acsearthspacechem.9b00195
ACS Earth Space Chem. 2019, 3, 2404−2414

semivolatile carboxylic acids is suppressed by high concentration of nitric acid.

4. CONCLUSIONS AND ATMOSPHERIC IMPLICATIONS

We conclude that the mechanistic role of mineral dust in SOA growth changes with the water content in dust particles. The formation of carboxylate salts modulates SOA growth with dry dust and the aqueous reactions enhance SOA growth with wet GDD. Figure 1 supports the enhancement of SOA growth by the formation of carboxylates in the presence of dry GDD particles. The mechanistic role of wet dust particles in SOA growth via heterogeneous reactions of organic compounds was discussed, as shown in Figure 6. Overall, SOA mass driven by gas-particle partitioning is relatively smaller than that geared by heterogeneous reactions. In addition, Figure 5 supports the influence of GDD on the degradation of an organic compound. SVOCs can be oxidized by the OH radicals that are generated via the photocatalytic activation of dust particles and form less volatile HOM compounds or more volatile IVOCs (see Section 3.3). Thus, dust-driven photocatalytic oxidation of organic compounds could influence both SOA growth and aerosol's chemical characteristics. The impact of photocatalytic oxidation on SOA needs to be further studied in future.

Laboratory studies showed that the hygroscopicity of dust particles can be modified via the heterogeneous reaction of SO_2 and NO_2.[32,83,84] In addition to NO_x and SO_2, HC is ubiquitous in heavily polluted urban environments and interacts with airborne dust particles. The coating of organic products on dust particles, that is, carboxylic acids, also modifies dust's hygroscopicity. In general, carboxylate salts are less hygroscopic than nitrate salts.[85] The modified hygroscopicity of dust particles further influences CCN activity,[86,87] ice nuclei,[88,89] and single-scattering albedo.[90] In addition, the effect of salts on the solubility of organic compounds in the water layer on dust particles can be diverse with ionic composition. For example, salting out of organic compounds with calcium nitrate is generally stronger than that with AS.[91]

As discussed in Section 3.4, the lifetime associated with the photocatalytic oxidation of SVOC ($P_L \leq 10^{-3}$ mm Hg) on GDD particles is significant under typical dust episode conditions (i.e., 400 μg m^{-3} dust loading at 50% RH).[25,26] A significant fraction of oxygenated products from the atmospheric processes of VOC precursors is SVOCs with $P_L \leq 10^{-3}$ mm Hg (i.e., 15−40% in toluene products under various NO_x and aging conditions).[36] Although the impact of dust particles on ozone formation was not apparent in our chamber studies, it is capable of the dust to modify SOA compositions through both gas-phase reaction and heterogeneous reactions.[92−95] In addition, NO_x can influence SOA formation by both gas-phase chemistry and dust-phase heterogeneous chemistry. For example, the SOA yield is usually lower with high NO_x conditions than that with low NO_x conditions.[33] NO_2 consumes the electron on dust particles to form NO[96] as well as HONO, which is the precursor of OH radicals.[97] In the heavily polluted urban regions located in the mid-latitude where the temperature climate is mild, RH is generally higher than 30%, and the concentration of aromatic VOC and NO_x can reach to ∼200 ppbC and ∼70 ppb, respectively.[98,99] Therefore, mineral dust can be easily nitrated in the urban areas and become more hygroscopic than fresh dust. SOA growth in the presence of wet dust particles will be driven by aqueous reactions of the reactive oxygenated products originating from the photooxidation of VOC. We conclude that SOA mass increases in the presence of mineral dust particles.

■ ASSOCIATED CONTENT

Supporting Information

The Supporting Information is available free of charge on the ACS Publications website at DOI: 10.1021/acsearthspacechem.9b00195.

Sample preparation of GDD-BZA and GDD-sodium benzoate; preparation of outdoor chamber experiments and experimental results; peak assignments in FTIR spectral data; estimation of the lifetime of organic products on dust; dust phase water content; and the concentration of nitrate in GDD particles in the presence of TMB (PDF)

■ AUTHOR INFORMATION

Corresponding Author

*E-mail: mjang@ufl.edu. Phone: +1-352-846-1744.

ORCID

Zechen Yu: 0000-0002-6763-0520

Myoseon Jang: 0000-0003-4211-7883

Author Contributions

The manuscript was written through the contributions of all authors. All authors have given approval to the final version of the manuscript.

Notes

The authors declare no competing financial interest.

■ ACKNOWLEDGMENTS

This research was supported by funding support from the National Science Foundation (NSF#1923651), the Ministry of Science and ICT, the Ministry of Environment, the Ministry of Health and Welfare (2017M3D8A1090654), the National Institute of Metrological Sciences (KMA2018-00512), and the Fulbright Scholarship (from USA to Mongolia).

■ REFERENCES

(1) Peng, Y.; von Salzen, K.; Li, J. Simulation of Mineral Dust Aerosol with Piecewise Log-normal Approximation (PLA) in CanAM4-PAM. *Atmos. Chem. Phys.* **2012**, *12*, 6891−6914.

(2) Textor, C.; Schulz, M.; Guibert, S.; Kinne, S.; Balkanski, Y.; Bauer, S.; Berntsen, T.; Berglen, T.; Boucher, O.; Chin, M.; Dentener, F.; Diehl, T.; Easter, R.; Feichter, H.; Fillmore, D.; Ghan, S.; Ginoux, P.; Gong, S.; Grini, A.; Hendricks, J.; Horowitz, L.; Huang, P.; Isaksen, I.; Iversen, I.; Kloster, S.; Koch, D.; Kirkevåg, A.; Kristjansson, J. E.; Krol, M.; Lauer, A.; Lamarque, J. F.; Liu, X.; Montanaro, V.; Myhre, G.; Penner, J.; Pitari, G.; Reddy, S.; Seland, Ø.; Stier, P.; Takemura, T.; Tie, X. Analysis and Quantification of the Diversities of Aerosol Life Cycles within AeroCom. *Atmos. Chem. Phys.* **2006**, *6*, 1777−1813.

(3) Ke-Yi, C. The Northern Path of Asian Dust Transport from the Gobi Desert to North America. *Atmos. Ocean. Sci. Lett.* **2010**, *3*, 155−159.

(4) Mogili, P. K.; Kleiber, P. D.; Young, M. A.; Grassian, V. H. Heterogeneous Uptake of Ozone on Reactive Components of Mineral Dust Aerosol: An Environmental Aerosol Reaction Chamber Study. *J. Phys. Chem. A* **2006**, *110*, 13799−13807.

(5) Usher, C. R.; Al-Hosney, H.; Carlos-Cuellar, S.; Grassian, V. H. A Laboratory Study of the Heterogeneous Uptake and Oxidation of Sulfur Dioxide on Mineral Dust Particles. *J. Geophys. Res.-Atmos.* **2002**, *107*, 16.

DOI: 10.1021/acsearthspacechem.9b00195
ACS Earth Space Chem. 2019, 3, 2404−2414

(6) Zhang, X.; Zhuang, G.; Chen, J.; Wang, Y.; Wang, X.; An, Z.; Zhang, P. Heterogeneous Reactions of Sulfur Dioxide on Typical Mineral Particles. *J. Phys. Chem. B* **2006**, *110*, 12588−12596.
(7) Dupart, Y.; King, S. M.; Nekat, B.; Nowak, A.; Wiedensohler, A.; Herrmann, H.; David, G.; Thomas, B.; Miffre, A.; Rairoux, P.; D'Anna, B.; George, C. Mineral Dust Photochemistry Induces Nucleation Events in the Presence of SO_2. *Proc. Natl. Acad. Sci. U.S.A.* **2012**, *109*, 20842−20847.
(8) El Zein, A.; Romanias, M. N.; Bedjanian, Y. Heterogeneous Interaction of H_2O_2 with Arizona Test Dust. *J. Phys. Chem. A* **2014**, *118*, 441−448.
(9) Yang, W.; Zhang, J.; Ma, Q.; Zhao, Y.; Liu, Y.; He, H. Heterogeneous Reaction of SO_2 on Manganese Oxides: the Effect of Crystal Structure and Relative Humidity. *Sci. Rep.* **2017**, *7*, 4550.
(10) Park, J. Y.; Jang, M. Heterogeneous Photooxidation of Sulfur Dioxide in the Presence of Airborne Mineral Dust Particles. *RSC Adv.* **2016**, *6*, 58617−58627.
(11) Yu, Z.; Jang, M.; Park, J. Modeling Atmospheric Mineral Aerosol Chemistry to Predict Heterogeneous Photooxidation of SO_2. *Atmos. Chem. Phys.* **2017**, *17*, 10001−10017.
(12) Ponczek, M.; George, C. Kinetics and Product Formation during the Photooxidation of Butanol on Atmospheric Mineral Dust. *Environ. Sci. Technol.* **2018**, *52*, 5191−5198.
(13) Al-Hosney, H. A.; Carlos-Cuellar, S.; Baltrusaitis, J.; Grassian, V. H. Heterogeneous Uptake and Reactivity of Formic Acid on Calcium Carbonate Particles: a Knudsen Cell Reactor, FTIR and SEM Study. *Phys. Chem. Chem. Phys.* **2005**, *7*, 3587−3595.
(14) Ma, Q.; Liu, Y.; Liu, C.; He, H. Heterogeneous Reaction of Acetic Acid on MgO, α-Al_2O_3, and $CaCO_3$ and the Effect on the Hygroscopic Behaviour of these Particles. *Phys. Chem. Chem. Phys.* **2012**, *14*, 8403−8409.
(15) Tang, M.; Larish, W. A.; Fang, Y.; Gankanda, A.; Grassian, V. H. Heterogeneous Reactions of Acetic Acid with Oxide Surfaces: Effects of Mineralogy and Relative Humidity. *J. Phys. Chem. A* **2016**, *120*, 5609−5616.
(16) Liu, C.; Chu, B.; Liu, Y.; Ma, Q.; Ma, J.; He, H.; Li, J.; Hao, J. Effect of Mineral Dust on Secondary Organic Aerosol Yield and Aerosol Size in Alpha-pinene/NO_x Photo-oxidation. *Atmos. Environ.* **2013**, *77*, 781−789.
(17) Chu, B.; Liu, T.; Zhang, X.; Liu, Y.; Ma, Q.; Ma, J.; He, H.; Wang, X.; Li, J.; Hao, J. Secondary Aerosol Formation and Oxidation Capacity in Photooxidation in the Presence of Al_2O_3 Seed Particles and SO_2. *Sci China Chem* **2015**, *58*, 1426−1434.
(18) Zhao, Y.; Huang, D.; Huang, L.; Chen, Z. Hydrogen Peroxide Enhances the Oxidation of Oxygenated Volatile Organic Compounds on Mineral Dust Particles: A Case Study of Methacrolein. *Environ. Sci. Technol.* **2014**, *48*, 10614−10623.
(19) Zeineddine, M. N.; Romanias, M. N.; Gaudion, V.; Riffault, V.; Thévenet, F. Heterogeneous Interaction of Isoprene with Natural Gobi Dust. *ACS Earth Space Chem* **2017**, *1*, 236−243.
(20) Jimenez, J. L.; Canagaratna, M. R.; Donahue, N. M.; Prevot, A. S. H.; Zhang, Q.; Kroll, J. H.; DeCarlo, P. F.; Allan, J. D.; Coe, H.; Ng, N. L.; Aiken, A. C.; Docherty, K. S.; Ulbrich, I. M.; Grieshop, A. P.; Robinson, A. L.; Duplissy, J.; Smith, J. D.; Wilson, K. R.; Lanz, V. A.; Hueglin, C.; Sun, Y. L.; Tian, J.; Laaksonen, A.; Raatikainen, T.; Rautiainen, J.; Vaattovaara, P.; Ehn, M.; Kulmala, M.; Tomlinson, J. M.; Collins, D. R.; Cubison, M. J.; Dunlea, J.; Huffman, J. A.; Onasch, T. B.; Alfarra, M. R.; Williams, P. I.; Bower, K.; Kondo, Y.; Schneider, J.; Drewnick, F.; Borrmann, S.; Weimer, S.; Demerjian, K.; Salcedo, D.; Cottrell, L.; Griffin, R.; Takami, A.; Miyoshi, T.; Hatakeyama, S.; Shimono, A.; Sun, J. Y.; Zhang, Y. M.; Dzepina, K.; Kimmel, J. R.; Sueper, D.; Jayne, J. T.; Herndon, S. C.; Trimborn, A. M.; Williams, L. R.; Wood, E. C.; Middlebrook, A. M.; Kolb, C. E.; Baltensperger, U.; Worsnop, D. R. Evolution of Organic Aerosols in the Atmosphere. *Science* **2009**, *326*, 1525−1529.
(21) Spracklen, D. V.; Jimenez, J. L.; Carslaw, K. S.; Worsnop, D. R.; Evans, M. J.; Mann, G. W.; Zhang, Q.; Canagaratna, M. R.; Allan, J.; Coe, H.; McFiggans, G.; Rap, A.; Forster, P. Aerosol Mass Spectrometer Constraint on the Global Secondary Organic Aerosol Budget. *Atmos. Chem. Phys.* **2011**, *11*, 12109−12136.
(22) Shrivastava, M.; Easter, R. C.; Liu, X.; Zelenyuk, A.; Singh, B.; Zhang, K.; Ma, P.-L.; Chand, D.; Ghan, S.; Jimenez, J. L.; Zhang, Q.; Fast, J.; Rasch, P. J.; Tiitta, P. Global Transformation and Fate of SOA: Implications of Low-volatility SOA and Gas-phase Fragmentation Reactions. *J Geophys Res-Atmos* **2015**, *120*, 4169−4195.
(23) Hodzic, A.; Kasibhatla, P. S.; Jo, D. S.; Cappa, C. D.; Jimenez, J. L.; Madronich, S.; Park, R. J. Rethinking the Global Secondary Organic Aerosol (SOA) Budget: Stronger Production, Faster Removal, Shorter Lifetime. *Atmos. Chem. Phys.* **2016**, *16*, 7917−7941.
(24) Wood, E. C.; Canagaratna, M. R.; Herndon, S. C.; Onasch, T. B.; Kolb, C. E.; Worsnop, D. R.; Kroll, J. H.; Knighton, W. B.; Seila, R.; Zavala, M.; Molina, L. T.; DeCarlo, P. F.; Jimenez, J. L.; Weinheimer, A. J.; Knapp, D. J.; Jobson, B. T.; Stutz, J.; Kuster, W. C.; Williams, E. J. Investigation of the Correlation between Odd Oxygen and Secondary Organic Aerosol in Mexico City and Houston. *Atmos. Chem. Phys.* **2010**, *10*, 8947−8968.
(25) Wang, G.; Cheng, C.; Meng, J.; Huang, Y.; Li, J.; Ren, Y. Field Observation on Secondary Organic Aerosols during Asian Dust Storm Periods: Formation Mechanism of Oxalic Acid and Related Compounds on Dust Surface. *Atmos. Environ.* **2015**, *113*, 169−176.
(26) Ren, Y. Q.; Wang, G. H.; Li, J. J.; Wu, C.; Cao, C.; Li, J.; Wang, J. Y.; Ge, S. S.; Xie, Y. N.; Li, X. R.; Meng, F.; Li, H. Evolution of Aerosol Chemistry in Xi'an During the Spring Dust Storm Periods: Implications for Heterogeneous Formation of Secondary Organic Aerosols on the Dust Surface. *Chemosphere* **2019**, *215*, 413−421.
(27) Mochizuki, T.; Kawamura, K.; Aoki, K.; Sugimoto, N. Long-range Atmospheric Transport of Volatile Monocarboxylic Acids with Asian Dust over a High Mountain Snow Site, Central Japan. *Atmos. Chem. Phys.* **2016**, *16*, 14621−14633.
(28) Park, J.; Jang, M.; Yu, Z. Heterogeneous Photo-oxidation of SO_2 in the Presence of Two Different Mineral Dust Particles: Gobi and Arizona Dust. *Environ. Sci. Technol.* **2017**, *51*, 9605−9613.
(29) Gustafsson, R. J.; Orlov, A.; Badger, C. L.; Griffiths, P. T.; Cox, R. A.; Lambert, R. M. A Comprehensive Evaluation of Water Uptake on Atmospherically Relevant Mineral Surfaces: DRIFT Spectroscopy, Thermogravimetric Analysis and Aerosol Growth Measurements. *Atmos. Chem. Phys.* **2005**, *5*, 3415−3421.
(30) Ibrahim, S.; Romanias, M. N.; Alleman, L. Y.; Zeineddine, M. N.; Angeli, G. K.; Trikalitis, P. N.; Thevenet, F. Water Interaction with Mineral Dust Aerosol: Particle Size and Hygroscopic Properties of Dust. *ACS Earth Space Chem.* **2018**, *2*, 376−386.
(31) Yu, Z.; Jang, M. Simulation of Heterogeneous Photooxidation of SO_2 and NO_x in the Presence of Gobi Desert Dust Particles Under Ambient Sunlight. *Atmos. Chem. Phys.* **2018**, *18*, 14609−14622.
(32) Tang, M.; Cziczo, D. J.; Grassian, V. H. Interactions of Water with Mineral Dust Aerosol: Water Adsorption, Hygroscopicity, Cloud Condensation, and Ice Nucleation. *Chem. Rev.* **2016**, *116*, 4205−4259.
(33) Hallquist, M.; Wenger, J. C.; Baltensperger, U.; Rudich, Y.; Simpson, D.; Claeys, M.; Dommen, J.; Donahue, N. M.; George, C.; Goldstein, A. H.; Hamilton, J. F.; Herrmann, H.; Hoffmann, T.; Iinuma, Y.; Jang, M.; Jenkin, M. E.; Jimenez, J. L.; Kiendler-Scharr, A.; Maenhaut, W.; McFiggans, G.; Mentel, T. F.; Monod, A.; Prévôt, A. S. H.; Seinfeld, J. H.; Surratt, J. D.; Szmigielski, R.; Wildt, J. The Formation, Properties and Impact of Secondary Organic Aerosol: Current and Emerging Issues. *Atmos. Chem. Phys.* **2009**, *9*, 5155−5236.
(34) McNeill, V. F. Aqueous Organic Chemistry in the Atmosphere: Sources and Chemical Processing of Organic Aerosols. *Environ. Sci. Technol.* **2015**, *49*, 1237−1244.
(35) Lim, Y. B.; Tan, Y.; Perri, M. J.; Seitzinger, S. P.; Turpin, B. J. Aqueous Chemistry and Its Role in Secondary Organic Aerosol (SOA) Formation. *Atmos. Chem. Phys.* **2010**, *10*, 10521−10539.
(36) Zhou, C.; Jang, M.; Yu, Z. Simulation of SOA Formation From the Photooxidation of Monoalkylbenzenes in the Presence of Aqueous Aerosols Containing Electrolytes Under Various NO_x Levels. *Atmos. Chem. Phys.* **2019**, *19*, 5719−5735.

DOI: 10.1021/acsearthspacechem.9b00195
ACS Earth Space Chem. 2019, 3, 2404−2414

(37) Im, Y.; Jang, M.; Beardsley, R. L. Simulation of Aromatic SOA Formation Using the Lumping Model Integrated with Explicit Gas-phase Kinetic Mechanisms and Aerosol-phase Reactions. *Atmos. Chem. Phys.* **2014**, *14*, 4013−4027.
(38) Jiang, H.; Jang, M.; Yu, Z. Dithiothreitol Activity by Particulate Oxidizers of SOA Produced from Photooxidation of Hydrocarbons under Varied NO_x Levels. *Atmos. Chem. Phys.* **2017**, *17*, 9965−9977.
(39) Yu, Z.; Jang, M.; Sabo-Attwood, T.; Robinson, S. E.; Jiang, H. Prediction of Delivery of Organic Aerosols onto Air-liquid Interface Cells in Vitro Using an Electrostatic Precipitator. *Toxicol. in Vitro* **2017**, *42*, 319−328.
(40) Chhabra, P. S.; Flagan, R. C.; Seinfeld, J. H. Elemental Analysis of Chamber Organic Aerosol using an Aerodyne High-resolution Aerosol Mass Spectrometer. *Atmos. Chem. Phys.* **2010**, *10*, 4111−4131.
(41) Aiken, A. C.; Decarlo, P. F.; Kroll, J. H.; Worsnop, D. R.; Huffman, J. A.; Docherty, K. S.; Ulbrich, I. M.; Mohr, C.; Kimmel, J. R.; Sueper, D.; Sun, Y.; Zhang, Q.; Trimborn, A.; Northway, M.; Ziemann, P. J.; Canagaratna, M. R.; Onasch, T. B.; Alfarra, M. R.; Prevot, A. S. H.; Dommen, J.; Duplissy, J.; Metzger, A.; Baltensperger, U.; Jimenez, J. L. O/C and OM/OC Ratios of Primary, Secondary, and Ambient Organic Aerosols with High-resolution Time-of-flight Aerosol Mass Spectrometry. *Environ. Sci. Technol.* **2008**, *42*, 4478−4485.
(42) Canagaratna, M. R.; Jimenez, J. L.; Kroll, J. H.; Chen, Q.; Kessler, S. H.; Massoli, P.; Hildebrandt Ruiz, L.; Fortner, E.; Williams, L. R.; Wilson, K. R.; Surratt, J. D.; Donahue, N. M.; Jayne, J. T.; Worsnop, D. R. Elemental Ratio Measurements of Organic Compounds using Aerosol Mass Spectrometry: Characterization, Improved Calibration, and Implications. *Atmos. Chem. Phys.* **2015**, *15*, 253−272.
(43) Febo, A.; Perrino, C. Prediction and experimental evidence for high air concentration of nitrous acid in indoor environments. *Atmos. Environ. a-Gen.* **1991**, *25*, 1055−1061.
(44) Jang, M.; Kamens, R. M. Characterization of Secondary Aerosol from the Photooxidation of Toluene in the Presence of NO_x and 1-Propene. *Environ. Sci. Technol.* **2001**, *35*, 3626−3639.
(45) Chien, C.-J.; Charles, M. J.; Sexton, K. G.; Jeffries, H. E. Analysis of Airborne Carboxylic Acids and Phenols as Their Pentafluorobenzyl Derivatives: Gas Chromatography/Ion Trap Mass Spectrometry with a Novel Chemical Ionization Reagent, PFBOH. *Environ. Sci. Technol.* **1998**, *32*, 299−309.
(46) Liu, T.; Huang, D. D.; Li, Z.; Liu, Q.; Chan, M.; Chan, C. K. Comparison of Secondary Organic Aerosol Formation from Toluene on Initially Wet and Dry Ammonium Sulfate Particles at Moderate Relative Humidity. *Atmos. Chem. Phys.* **2018**, *18*, 5677−5689.
(47) Beardsley, R. L.; Jang, M. Simulating the SOA Formation of Isoprene from Partitioning and Aerosol Phase Reactions in the Presence of Inorganics. *Atmos. Chem. Phys.* **2016**, *16*, 5993−6009.
(48) Clegg, S. L.; Brimblecombe, P.; Wexler, A. S. Thermodynamic Model of the System H^+-NH_4^+-SO_4^{2-}-NO_3^--H_2O at Tropospheric Temperatures. *J. Phys. Chem. A* **1998**, *102*, 2137−2154.
(49) Wexler, A. S.; Clegg, S. L. Atmospheric Aerosol Models for Systems Including the Ions H^+, NH_4^+, Na^+, SO_4^{2-}, NO_3^-, Cl^-, Br^-, and H_2O. *J. Geophys. Res.: Atmos.* **2002**, *107*, 4207.
(50) Clegg, S. L.; Wexler, A. S. Densities and Apparent Molar Volumes of Atmospherically Important Electrolyte Solutions. 2. The Systems H^+− HSO_4^-− SO_4^{2-}− H_2O from 0 to 3 mol kg^{-1} as a Function of Temperature and H^+− NH_4^+− HSO_4^-− SO_4^{2-}− H_2O from 0 to 6 mol kg^{-1} at 25° C Using a Pitzer Ion Interaction Model, and NH_4HSO_4− H_2O and $(NH_4)_3H(SO_4)_2$− H_2O over the Entire Concentration Range. *J. Phys. Chem. A* **2011**, *115*, 3461−3474.
(51) Nenes, A.; Pandis, S. N.; Pilinis, C. ISORROPIA: A New Thermodynamic Equilibrium Model for Multiphase Multicomponent Inorganic Aerosols. *Aquat. Geochem.* **1998**, *4*, 123−152.
(52) Fountoukis, C.; Nenes, A. ISORROPIA II: a Computationally Efficient Thermodynamic Equilibrium Model for K^+-Ca^{2+}-Mg^{2+}-NH_4^+-Na^+-SO_4^{2-}-NO_3^--Cl^--H_2O Aerosols. *Atmos. Chem. Phys.* **2008**, *7*, 4639−4659.
(53) Al-Hosney, H. A.; Grassian, V. H. Water, Sulfur Dioxide and Nitric Acid Adsorption on Calcium Carbonate: A Transmission and ATR-FTIR Study. *Phys. Chem. Chem. Phys.* **2005**, *7*, 1266−1276.
(54) Liu, Y. J.; Zhu, T.; Zhao, D. F.; Zhang, Z. F. Investigation of the Hygroscopic Properties of $Ca(NO_3)_2$ and Internally Mixed Ca-$(NO_3)_2$/$CaCO_3$ Particles by Micro-Raman Spectrometry. *Atmos. Chem. Phys.* **2008**, *8*, 7205−7215.
(55) Beardsley, R.; Jang, M.; Ori, B.; Im, Y.; Delcomyn, C. A.; Witherspoon, N. Role of Sea Salt Aerosols in the Formation of Aromatic Secondary Organic Aerosol: Yields and Hygroscopic Properties. *Environ. Chem.* **2013**, *10*, 167−177.
(56) Abdelkader, M.; Metzger, S.; Steil, B.; Klingmüller, K.; Tost, H.; Pozzer, A.; Stenchikov, G.; Barrie, L.; Lelieveld, J. Sensitivity of Transatlantic Dust Transport to Chemical Aging and Related Atmospheric Processes. *Atmos. Chem. Phys.* **2017**, *17*, 3799−3821.
(57) Nah, T.; Mcvay, R. C.; Zhang, X.; Boyd, C. M.; Seinfeld, J. H.; Ng, N. L. Influence of Seed Aerosol Surface Area and Oxidation Rate on Vapor Wall Deposition and SOA Mass Yields: A Case Study with Alpha-pinene Ozonolysis. *Atmos. Chem. Phys.* **2016**, *16*, 9361−9379.
(58) Ahlberg, E.; Eriksson, A.; Brune, W. H.; Roldin, P.; Svenningsson, B. Effect of Salt Seed Particle Surface Area, Composition and Phase on Secondary Organic Aerosol Mass Yields in Oxidation Flow Reactors. *Atmos. Chem. Phys.* **2019**, *19*, 2701−2712.
(59) Falkovich, A. H.; Schkolnik, G.; Ganor, E.; Rudich, Y. Adsorption of Organic Compounds Pertinent to Urban Environments onto Mineral Dust Particles. *J. Geophys. Res.-Atmos.* **2004**, *109*, D02208.
(60) Shen, X.; Zhao, Y.; Chen, Z.; Huang, D. Heterogeneous Reactions of Volatile Organic Compounds in the Atmosphere. *Atmos. Environ.* **2013**, *68*, 297−314.
(61) Liu, Q.; Liggio, J.; Breznan, D.; Thomson, E. M.; Kumarathasan, P.; Vincent, R.; Li, K.; Li, S.-M. Oxidative and Toxicological Evolution of Engineered Nanoparticles with Atmospherically Relevant Coatings. *Environ. Sci. Technol.* **2019**, *53*, 3058−3066.
(62) Gankanda, A.; Grassian, V. H. Nitrate Photochemistry on Laboratory Proxies of Mineral Dust Aerosol: Wavelength Dependence and Action Spectra. *J. Phys. Chem. C* **2014**, *118*, 29117−29125.
(63) Dupart, Y.; Fine, L.; D'Anna, B.; George, C. Heterogeneous Uptake of NO_2 on Arizona Test Dust under UV-A Irradiation: An Aerosol Flow Tube Study. *Aeolian Res.* **2014**, *15*, 45−51.
(64) Vlasenko, A.; Sjogren, S.; Weingartner, E.; Stemmler, K.; Gäggeler, H. W.; Ammann, M. Effect of Humidity on Nitric Acid Uptake to Mineral Dust Aerosol Particles. *Atmos. Chem. Phys.* **2006**, *6*, 2147−2160.
(65) Matsuki, A.; Iwasaka, Y.; Shi, G.; Zhang, D.; Trochkine, D.; Yamada, M.; Kim, Y.-S.; Chen, B.; Nagatani, T.; Miyazawa, T.; Nagatani, M.; Nakata, H. Morphological and Chemical Modification of Mineral Dust: Observational Insight into the Heterogeneous Uptake of Acidic Gases. *Geophys. Res. Lett.* **2005**, *32*, a.
(66) Scheuvens, D.; Schütz, L.; Kandler, K.; Ebert, M.; Weinbruch, S. Bulk Composition of Northern African Dust and Its Source Sediments - A Compilation. *Earth-Sci. Rev.* **2013**, *116*, 170−194.
(67) Al-Dousari, A. M.; Al-Awadhi, J.; Ahmed, M. Dust Fallout Characteristics within Global Dust Storm Major Trajectories. *Arab. J. Geosci.* **2013**, *6*, 3877−3884.
(68) Wang, B.; Laskin, A. Reactions between Water-soluble Organic Acids and Nitrates in Atmospheric Aerosols: Recycling of Nitric Acid and Formation of Organic Salts. *J. Geophys. Res.-Atmos.* **2014**, *119*, 3335−3351.
(69) Yarwood, G.; Jung, J.; Whitten, G. Z.; Heo, G.; Mellberg, J.; Estes, M. In *Updates to the Carbon Bond Mechanism for Version 6 (CB6), 2010 CMAS Conference*: Chapel Hill, NC, Oct 2010, http://www.cmascenter.org/conference/2010/abstracts/emery_updates_carbon_2010.pdf.
(70) Emmerson, K. M.; Evans, M. J. Comparison of Tropospheric Gas-phase Chemistry Schemes for Use within Global Models. *Atmos. Chem. Phys.* **2009**, *9*, 1831−1845.

DOI: 10.1021/acsearthspacechem.9b00195
ACS Earth Space Chem. 2019, 3, 2404−2414

(71) Hoffmann, M.; Calvert, J. The Aqueous Phase Chemistry. In *Chemical Transformation Modules for Eulerian Acid Deposition Models*; National Center for Atmospheric Research Boulder: CO, 1985; Vol. *2*, pp 147−189.
(72) Thompson, T. L.; Yates, J. T. Surface science studies of the photoactivation of TiO_2 new photochemical processes. *Chem. Rev.* **2006**, *106*, 4428−4453.
(73) George, C.; Ammann, M.; D'Anna, B.; Donaldson, D. J.; Nizkorodov, S. A. Heterogeneous Photochemistry in the Atmosphere. *Chem. Rev.* **2015**, *115*, 4218−4258.
(74) Huang, L.; Zhao, Y.; Li, H.; Chen, Z. Kinetics of Heterogeneous Reaction of Sulfur Dioxide on Authentic Mineral Dust: Effects of Relative Humidity and Hydrogen Peroxide. *Environ. Sci. Technol.* **2015**, *49*, 10797−10805.
(75) Chen, Y.; Tong, S.; Wang, J.; Peng, C.; Ge, M.; Xie, X.; Sun, J. Effect of Titanium Dioxide on Secondary Organic Aerosol Formation. *Environ. Sci. Technol.* **2018**, *52*, 11612−11620.
(76) Usher, C.; Michel, A. E.; Stec, D.; Grassian, V. H. Laboratory Studies of Ozone Uptake on Processed Mineral Dust. *Atmos. Environ.* **2003**, *37*, 5337−5347.
(77) Chang, R. Y.-W.; Sullivan, R. C.; Abbatt, J. P. D. Initial Uptake of Ozone on Saharan Dust at Atmospheric Relative Humidities. *Geophys. Res. Lett.* **2005**, *32*, L14815.
(78) Wang, S.; Ackermann, R.; Spicer, C. W.; Fast, J. D.; Schmeling, M.; Stutz, J. Atmospheric Observations of Enhanced NO_2-HONO Conversion on Mineral Dust Particles. *Geophys. Res. Lett.* **2003**, *30*, 1595.
(79) Ndour, M.; D'Anna, B.; George, C.; Ka, O.; Balkanski, Y.; Kleffmann, J.; Stemmler, K.; Ammann, M. Photoenhanced Uptake of NO_2 on Mineral Dust: Laboratory Experiments and Model Simulations. *Geophys. Res. Lett.* **2008**, *35*, L05812.
(80) Scheuvens, D.; Kandler, K. On Composition, Morphology, and Size Distribution of Airborne Mineral Dust. In *Mineral Dust: A Key Player in the Earth System*; Knippertz, P., Stuut, J.-B. W., Eds.; Springer Netherlands: Dordrecht, 2014; pp 15−49.
(81) Zender, C. S.; Miller, R. L. R. L.; Tegen, I. Quantifying Mineral Dust Mass Budgets:Terminology, Constraints, and Current Estimates. *Eos, Trans. Am. Geophys. Union* **2004**, *85*, 509−512.
(82) Weast, R. C.; Astle, M. J.; Beyer, W. H. *CRC Handbook of Chemistry and Physics*; CRC Press: Boca Raton, FL, 1988; Vol. *69*.
(83) Tang, M.; Huang, X.; Lu, K.; Ge, M.; Li, Y.; Cheng, P.; Zhu, T.; Ding, A.; Zhang, Y.; Gligorovski, S.; Song, W.; Ding, X.; Bi, X.; Wang, X. Heterogeneous Reactions of Mineral Dust Aerosol: Implications for Tropospheric Oxidation Capacity. *Atmos. Chem. Phys.* **2017**, *17*, 11727−11777.
(84) Jang, M.; Yu, Z. Modeling Heterogeneous Oxidation of NO_x, SO_2 and Hydrocarbons in the Presence of Mineral Dust Particles under Various Atmospheric Environments. *Multiphase Environmental Chemistry in the Atmosphere*; American Chemical Society, 2018; Vol. *1299*, pp 301−326.
(85) Drozd, G.; Woo, J.; Häkkinen, S. A. K.; Nenes, A.; McNeill, V. F. Inorganic Salts Interact with Oxalic Acid in Submicron Particles to Form Material with Low Hygroscopicity and Volatility. *Atmos. Chem. Phys.* **2014**, *14*, 5205−5215.
(86) Sullivan, R. C.; Moore, M. J. K.; Petters, M. D.; Kreidenweis, S. M.; Roberts, G. C.; Prather, K. A. Effect of Chemical Mixing State on the Hygroscopicity and Cloud Nucleation Properties of Calcium Mineral Dust Particles. *Atmos. Chem. Phys.* **2009**, *9*, 3303−3316.
(87) Karydis, V. A.; Tsimpidi, A. P.; Bacer, S.; Pozzer, A.; Nenes, A.; Lelieveld, J. Global Impact of Mineral Dust on Cloud Droplet Number Concentration. *Atmos. Chem. Phys.* **2017**, *17*, 5601−5621.
(88) Crawford, I.; Bower, K. N.; Choularton, T. W.; Dearden, C.; Crosier, J.; Westbrook, C.; Capes, G.; Coe, H.; Connolly, P. J.; Dorsey, J. R.; Gallagher, M. W.; Williams, P.; Trembath, J.; Cui, Z.; Blyth, A. Ice Formation and Development in Aged, Wintertime Cumulus over the UK: Observations and Modelling. *Atmos. Chem. Phys.* **2012**, *12*, 4963−4985.
(89) Chen, J.-P.; Hazra, A.; Levin, Z. Parameterizing Ice Nucleation Rates using Contact Angle and Activation Energy Derived from Laboratory Data. *Atmos. Chem. Phys.* **2008**, *8*, 7431−7449.
(90) Bauer, S. E.; Mishchenko, M. I.; Lacis, A. A.; Zhang, S.; Perlwitz, J.; Metzger, S. M. Do Sulfate and Nitrate Coatings on Mineral Dust have Important Effects on Radiative Properties and Climate Modeling? *J. Geophys. Res.: Atmos.* **2007**, *112*, D06307.
(91) Görgényi, M.; Dewulf, J.; Van Langenhove, H.; Héberger, K. Aqueous Salting-out Effect of Inorganic Cations and Anions on Non-electrolytes. *Chemosphere* **2006**, *65*, 802−810.
(92) Epstein, S. A.; Blair, S. L.; Nizkorodov, S. A. Direct Photolysis of α-Pinene Ozonolysis Secondary Organic Aerosol: Effect on Particle Mass and Peroxide Content. *Environ. Sci. Technol.* **2014**, *48*, 11251−11258.
(93) Fuentes, Z. L. C.; Kucinski, T. M.; Hinrichs, R. Z. Ozone Decomposition on Kaolinite as a Function of Monoterpene Exposure and Relative Humidity. *ACS Earth Space Chem.* **2018**, *2*, 21−30.
(94) Chen, L.; Zheng, C.; Gao, X.; Cen, K.; Bao, K.; Li, K.; Lv, B.; Bao, Z.; Lin, C.; Wu, X. Ozone and Secondary Organic Aerosol Formation of Toluene/NOx Irradiations under Complex Pollution Scenarios. *Aerosol Air Qual. Res.* **2017**, *17*, 1760−1771.
(95) Chen, F.; Zhou, H.; Gao, J.; Hopke, P. K. A Chamber Study of Secondary Organic Aerosol (SOA) Formed by Ozonolysis of d-Limonene in the Presence of NO. *Aerosol Air Qual. Res.* **2017**, *17*, 59−68.
(96) Styler, S. A.; Donaldson, D. J. Photooxidation of Atmospheric Alcohols on Laboratory Proxies for Mineral Dust. *Environ. Sci. Technol.* **2011**, *45*, 10004−10012.
(97) Saliba, N. A.; Moussa, S. G.; El Tayyar, G. Contribution of Airborne Dust Particles to HONO Sources. *Atmos. Chem. Phys. Disc.* **2014**, *14*, 4827−4839.
(98) Khan, A.; Szulejko, J. E.; Kim, K.-H.; Brown, R. J. C. Airborne volatile aromatic hydrocarbons at an urban monitoring station in Korea from 2013 to 2015. *J. Environ. Manage.* **2018**, *209*, 525−538.
(99) Gao, Y.; Wang, H.; Zhang, X.; Jing, S. a.; Peng, Y.; Qiao, L.; Zhou, M.; Huang, D. D.; Wang, Q.; Li, X.; Li, L.; Feng, J.; Ma, Y.; Li, Y. Estimating Secondary Organic Aerosol Production from Toluene Photochemistry in a Megacity of China. *Environ. Sci. Technol.* **2019**, *53*, 8664−8671.

DOI: 10.1021/acsearthspacechem.9b00195
ACS Earth Space Chem. 2019, 3, 2404−2414